

**Short- and intermediate-range structure of liquid GeSe<sub>2</sub>**Carlo Massobrio,<sup>1</sup> Alfredo Pasquarello,<sup>2</sup> and Roberto Car<sup>3</sup><sup>1</sup>*Institut de Physique et de Chimie des Matériaux de Strasbourg, 23 rue du Loess, F-67037 Strasbourg, France*<sup>2</sup>*Institut Romand de Recherche Numérique en Physique des Matériaux (IRRMA), Ecole Polytechnique Fédérale de Lausanne (EPFL), PPH-Ecublens, CH-1015 Lausanne, Switzerland*<sup>3</sup>*Department of Chemistry and Princeton Materials Institute, Frick Chemical Laboratory, Washington Road, Princeton University, Princeton, New Jersey 08544*

(Received 3 May 2001; published 24 September 2001)

First-principles molecular dynamics simulations are carried out to study the structural properties of liquid GeSe<sub>2</sub>. We use a generalized gradient approximation for the exchange and correlation energy, which we find to improve significantly upon the local density approximation in describing both the short- and the intermediate-range structure. A very good agreement with experiment is obtained for the total neutron structure factor over the entire range of momentum transfer. In particular, the first sharp diffraction peak (FSDP) is well reproduced. We carry out a detailed comparison between partial structure factors and partial pair correlations in theory and experiment to assess the quality of our simulation model. The short-range and intermediate-range structure are well described overall. However, residual differences between theory and experiment, such as the absence of a FSDP in the concentration-concentration structure factor, appear and are traced back to the Ge-Ge correlations. An analysis of the bonding configurations indicates that liquid GeSe<sub>2</sub> is a defective network consisting of predominant Ge-centered tetrahedral units, but Ge- and Se-centered triads and homopolar bonds occur in non-negligible amounts. The number of Ge—Ge homopolar bonds and of ordered fourfold rings compare favorably with experimental estimates. Chemical disorder manifests through an important percentage of Se-rich odd-membered rings. We characterized the intermediate-range order by studying the relation between real-space distances and the FSDP. We found that this feature appears when correlations beyond 5 Å are accounted for. The evaluation of bond lifetimes reflect the higher stability of Ge—Se bonds with respect to homopolar bonds, consistent with the predominance of tetrahedral units.

DOI: 10.1103/PhysRevB.64.144205

PACS number(s): 61.25.Em, 61.20.Ja, 71.15.Pd

**I. INTRODUCTION**

Two contiguous length scales describe the amount of residual structural organization in a topologically disordered system.<sup>1</sup> On the one hand, short-range order (SRO) refers to correlations existing between nearest neighbors and is a common feature of most noncrystalline materials. On the other hand, intermediate- (also termed medium) range order (IRO) is defined as the level of structural organization involving distances significantly longer than nearest-neighbor bonds.<sup>1</sup> Network-forming liquids and glasses of stoichiometry AX<sub>2</sub> (A = Si, Ge; X = O, S, Se) exhibit IRO through the appearance of a first sharp diffraction peak (FSDP) in the total neutron structure factor. This signature lies at a value of the momentum transfer  $k$  which typically corresponds to half the momentum transfer of the principal diffraction peak.<sup>2–4</sup>

Disordered GeSe<sub>2</sub> systems have often been selected as good prototypes to gain insight into the microscopic origin of the IRO.<sup>5–11</sup> From the structural point of view, this interest stems from two kinds of early observations. At variance with the case of SiO<sub>2</sub>, the chemical order in amorphous GeSe<sub>2</sub> was found to be broken, as proved by the finite concentration of Ge—Ge and Se—Se homopolar bonds.<sup>7,8</sup> These results have been confirmed very recently by further experimental work.<sup>12,13</sup> Moreover, in neutron diffraction experiments on liquid and glassy GeSe<sub>2</sub>, the FSDP was found to persist in the liquid with an intensity comparable to that of the glass, indicating that the IRO is preserved on melting.<sup>14</sup>

Molecular dynamics simulations based on classical inter-

atomic potentials were first employed to address key issues such as the nature of the network connectivity in terms of corner-sharing and edge-sharing tetrahedra and the extent of structural correlations in glassy and liquid GeSe<sub>2</sub>.<sup>15,16</sup> The use of these potentials gave a structure for liquid GeSe<sub>2</sub> devoid of homopolar bonds and a relative number of corner- and edge-sharing tetrahedra sensitively dependent on the consideration of three-body terms. These simulations were nevertheless able to reproduce satisfactorily the total neutron diffraction data, including the FSDP. By relying on a simplified model consisting of charged hard spheres, Iyetomi, Vashishta, and Kalia concluded that the FSDP in the total structure factor arises from a combination of steric and charge effects, which ensure the establishment of a regular network of tetrahedra.<sup>17</sup> Moreover, these authors suggested the absence of the FSDP in the charge-charge structure factor  $S_{zz}$  to be a generic property of any binary AX<sub>2</sub> disordered system.<sup>18</sup> On the experimental side, Penfold and Salmon questioned the validity of these assertions by carrying out a full partial-structure-factor analysis on liquid GeSe<sub>2</sub> with the method of isotopic substitution in neutron diffraction.<sup>19</sup> The partial pair correlation functions of liquid GeSe<sub>2</sub> were found to be consistent with the presence of Ge—Ge and Se—Se bonds which disrupt the chemical order of the network structure. In particular, a FSDP appeared in the Bhatia-Thornton<sup>20</sup> (BT) concentration-concentration structure factor  $S_{cc}$ , indicating concentration fluctuations over intermediate-range distances. This result is in marked contrast with the predictions of the classical molecular dynamics models,<sup>15–18</sup> pro-

vided the  $S_{zz}$  and  $S_{cc}$  structure factors are considered equivalent, as would be the case for a liquid with purely ionic species.

In previous work, we showed that the total structure factor of liquid  $\text{GeSe}_2$  obtained within a density functional approach accurately reproduces neutron diffraction data.<sup>21</sup> In particular, we demonstrated a relation between the degree of ionicity and the establishment of the IRO.<sup>22</sup> In this paper, we present a detailed description of the structural and dynamical properties of liquid  $\text{GeSe}_2$ . To this end, we here rely on a new set of extended first-principles molecular dynamics simulations using two different functionals for the exchange and correlation energy. First, we demonstrate the reliability of our model simulation by performing a close comparison with experimental data in reciprocal and real space. In particular, we found that the partial structure factors and pair correlation functions obtained within a generalized gradient approximation (GGA) significantly improve upon those obtained within the local density approximation (LDA). We then provide a detailed picture of the short- and intermediate-range structure. The structure of the liquid is characterized in terms of average coordination numbers, bond angle distributions, and ring statistics. Furthermore, we specifically address the IRO by establishing a relationship between the FSDP and the range of distances which account for its appearance. The dynamical behavior of the liquid is studied through the calculation of the diffusion coefficients and the bond lifetimes.

Our paper is organized as follows. In Sec. II we describe our simulation method and provide technical details. Sec. III is devoted to a comparison between experimental and theoretical partial structure factors and pair correlation functions. In particular, we compare the results obtained within the GGA and LDA schemes. Section IV is divided into three parts. In the first part, an analysis of the atomic configurations is given in terms of average coordination numbers and bond angle distributions. We then focus on the statistics of rings. In the last part of this section, we determine the range of interatomic distances which account for the appearance of the FSDP in the structure factors. Results on dynamical properties, including diffusion coefficients and bond lifetimes, are given in Sec. V. The paper concludes with Sec. VI.

## II. THEORETICAL MODEL

Our simulations were performed at constant volume on a system consisting of 120 atoms (40 Ge and 80 Se). We used a periodically repeated cubic cell of size  $15.7 \text{ \AA}$ , corresponding to the experimental density of the liquid at  $T=1050 \text{ K}$ . This system size is sufficiently large to cover the region of wave vectors in which the FSDP occurs. The smallest wave vector compatible with our supercell is  $k_{\min}=0.4 \text{ \AA}^{-1}$ , significantly smaller than the FSDP wave vector  $k_{\text{FSDP}}=1 \text{ \AA}^{-1}$  (Ref. 19). The region of wave vectors in which the FSDP appears is described by as much as eight discrete wavevectors compatible with the periodicity of our supercell.

The electronic structure was described within density functional theory (DFT) and evolved self-consistently during the motion.<sup>23</sup> We considered two distinct approximations for

the treatment of the exchange and correlation energy. The first approximation was the LDA, for which we used the results by Ceperley and Alder,<sup>24</sup> as interpolated by Perdew and Zunger<sup>25</sup>. The second one was the GGA introduced by Perdew *et al.*<sup>26</sup> Valence electrons were treated explicitly, in conjunction with norm-conserving pseudopotentials to account for core-valence interactions. The LDA pseudopotentials were taken from Ref. 27, while the GGA ones were generated as in Ref. 28.

The wave functions were expanded at the  $\Gamma$  point of the supercell on a plane-wave basis set defined by an energy cutoff  $E_c$ . In a first series of simulations, described in Ref. 21 and Ref. 22,  $E_c$  was taken equal to 10 Ry. We tested this choice on the Ge-Se dimer, finding bond lengths ( $d_0=4.06$  bohrs, for both the LDA and GGA) and vibrational frequencies ( $\omega=392 \text{ cm}^{-1}$  in the LDA,  $\omega=405 \text{ cm}^{-1}$  in the GGA), reproducing the experimental data<sup>29</sup> to within at most 1% and 4%, respectively. These dimer properties were found to be essentially converged for  $E_c=10 \text{ Ry}$ . In fact, increasing the cutoff  $E_c$  to 20 Ry led to negligible changes ( $d_0=4.08$  bohrs and  $\omega=392 \text{ cm}^{-1}$  in the GGA). In this paper, we nevertheless adopt a cutoff of  $E_c=20 \text{ Ry}$  for both the LDA and GGA simulations, because we found that this higher cutoff has the effect of moderately enhancing the ionicity of the system, thereby slightly improving the agreement with the experimental partial structure factors.<sup>30</sup>

The last configurations of the fully equilibrated trajectory

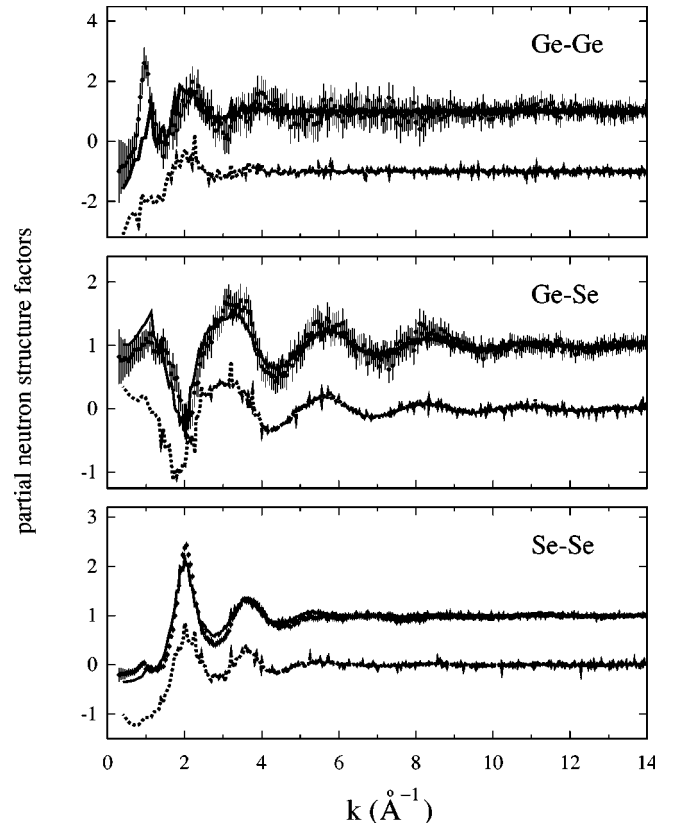


FIG. 1. Faber-Ziman partial structure factors for liquid  $\text{GeSe}_2$ : GGA calculations (solid line), LDA calculations (dotted line), and experiment (dots with error bars) (Ref. 19).  $S_{\text{GeGe}}^{\text{LDA}}(k)$ ,  $S_{\text{GeSe}}^{\text{LDA}}(k)$ , and  $S_{\text{SeSe}}^{\text{LDA}}(k)$  have been shifted down by 2, 1, and 1, respectively.

TABLE I. Positions ( $p$ ) and heights ( $h$ ) of the first maximum M1, first minimum m1, and second maximum M2 in the Faber-Ziman and Bhatia-Thornton partial structure factors. Positions are given in Å. In the absence of a signature, clearly discernible from the statistical noise, no data are reported. Error bars are the standard deviations from the mean for subaverages of 2 ps and 1 ps for the GGA and LDA simulations, respectively. The experimental results (expt) are taken from Refs. 19,37, and 38.

	$p$ -M1	$h$ -M1	$p$ -m1	$h$ -m1	$p$ -M2	$h$ -M2
$S_{GeGe}^{LDA}(k)$	-	-	-	-	2.04	$1.72 \pm 0.10$
$S_{GeGe}^{GGA}(k)$	1.13	$1.26 \pm 0.28$	1.27	$-0.13 \pm 0.06$	1.88	$1.85 \pm 0.20$
$S_{GeGe}^{expt}(k)$	0.98	$2.60 \pm 0.53$	1.45	$-0.50 \pm 0.41$	2.20	$1.98 \pm 0.51$
$S_{GeSe}^{LDA}(k)$	-	-	1.70	$-0.12 \pm 0.08$	2.86	$1.40 \pm 0.06$
$S_{GeSe}^{GGA}(k)$	1.13	$1.53 \pm 0.06$	2.00	$-0.33 \pm 0.10$	3.00	$1.44 \pm 0.02$
$S_{GeSe}^{expt}(k)$	1.00	$1.10 \pm 0.16$	1.95	$-0.14 \pm 0.21$	3.05	$1.68 \pm 0.22$
$S_{SeSe}^{LDA}(k)$	-	-	-	-	2.00	$1.85 \pm 0.10$
$S_{SeSe}^{GGA}(k)$	-	-	-	-	2.00	$2.17 \pm 0.14$
$S_{SeSe}^{expt}(k)$	0.95	$0.04 \pm 0.07$	1.15	$-0.12 \pm 0.06$	2.05	$2.43 \pm 0.07$
$S_{NN}^{LDA}(k)$	0.90	$0.48 \pm 0.04$	1.39	$0.35 \pm 0.04$	2.26	$1.13 \pm 0.10$
$S_{NN}^{GGA}(k)$	1.13	$0.81 \pm 0.06$	1.50	$0.42 \pm 0.02$	2.04	$1.06 \pm 0.03$
$S_{NN}^{expt}(k)$	1.00	$0.76 \pm 0.14$	1.35	$0.40 \pm 0.17$	2.00	$1.13 \pm 0.19$
$S_{NC}^{LDA}(k)$	0.90	$0.13 \pm 0.01$	2.0	$-0.14 \pm 0.02$	3.07	$0.06 \pm 0.01$
$S_{NC}^{GGA}(k)$	1.13	$0.21 \pm 0.02$	2.0	$-0.22 \pm 0.03$	2.92	$0.07 \pm 0.01$
$S_{NC}^{expt}(k)$	1.00	$0.27 \pm 0.05$	2.0	$-0.27 \pm 0.07$	2.70	$0.09 \pm 0.08$
$S_{CC}^{LDA}(k)$	-	-	-	-	2.00	$0.39 \pm 0.02$
$S_{CC}^{GGA}(k)$	-	-	-	-	2.04	$0.41 \pm 0.01$
$S_{CC}^{expt}(k)$	0.95	$0.25 \pm 0.04$	1.45	$0.09 \pm 0.04$	2.05	$0.45 \pm 0.05$

ries obtained in Refs. 21 and 22 for liquid GeSe<sub>2</sub> with  $E_c = 10$  Ry within the LDA and GGA schemes were taken as initial sets of coordinates for the simulations with  $E_c = 20$  Ry. We used a fictitious electron mass of  $\mu_0 = 5000$  a.u. (i.e., in units of  $m_e a_0^2$ , where  $m_e$  is the electronic mass and  $a_0$  is the Bohr radius) and a time step of  $\delta t = 0.54$  fs to integrate the equations of motion. To permit the use of such a large time step, we adopted the preconditioning scheme in Ref. 31 with a preconditioning cutoff of  $E_p = 3$  Ry. Temperature control is implemented for both ionic and electronic degrees of freedom by using Nosé-Hoover thermostats.<sup>32,33</sup> We carried out simulations at  $T = (1040 \pm 10)$  K over time periods of 9 ps and 21 ps for the LDA and GGA, respectively. When taking statistical averages, the initial segments of 1 ps for each of the two runs were discarded. The simulations were performed using for norm-conserving pseudopotentials the computer program described in Refs. 34 and 35.

### III. COMPARISON BETWEEN EXPERIMENT AND THEORY

#### A. Structure factors

The total neutron structure factors calculated with  $E_c = 20$  Ry do not differ significantly from those reported previously<sup>22,30</sup> and are not reproduced here. Besides a slight displacement of the FSDP towards larger  $k$  values, an overall very good agreement is found between the experimental total structure factor<sup>14</sup> and the theoretical one obtained within the GGA. At variance, the LDA total structure factor features a

much worse agreement, and, in particular, no FSDP appears. Therefore, in the following of this subsection, we first use the GGA results in the comparison between theory and experiment. For completeness, we then discuss the differences which arise within the LDA.

In Fig. 1, we display calculated and experimental Faber-Ziman<sup>36</sup> (FZ) partial structure factors. Relevant peak positions and heights are given in Table I. The experimental partial structure factor  $S_{GeGe}^{expt}(k)$  shows a very prominent FSDP, a lower second maximum, and two minima in the interval  $1.5 \text{ \AA}^{-1} < k < 4 \text{ \AA}^{-1}$  having close depths. The theoretical  $S_{GeGe}^{GGA}(k)$  compares favorably to the experimental  $S_{GeGe}^{expt}(k)$  but is less structured and shows a smaller FSDP. As in the total structure factor, the FSDP is displaced to larger  $k$  values by  $0.15 \text{ \AA}^{-1}$ . In the interval  $1.5 \text{ \AA}^{-1} < k < 3 \text{ \AA}^{-1}$ , the theoretical  $S_{GeGe}^{GGA}(k)$  is found to be slightly shifted towards smaller wave vectors with respect to the experimental curve. Calculated averages of the FSDP height on time periods of 2 ps are found to be strongly time dependent, leading to a theoretical error bar as large as 20%. However, despite these fluctuations, the height of the theoretical FSDP remains clearly below the experimental value.

The theoretical Ge-Se structure factor  $S_{GeSe}^{GGA}(k)$  reproduces accurately the data of Ref. 19 for  $k > 2 \text{ \AA}^{-1}$ , but for lower  $k$  values a small overall displacement is observed. Although the deviation is less striking than for Ge-Ge correlations, the theoretical FSDP in the Ge-Se structure factor is found to overestimate the experimental FSDP. Among the three Faber-Ziman structure factors, the best agreement with

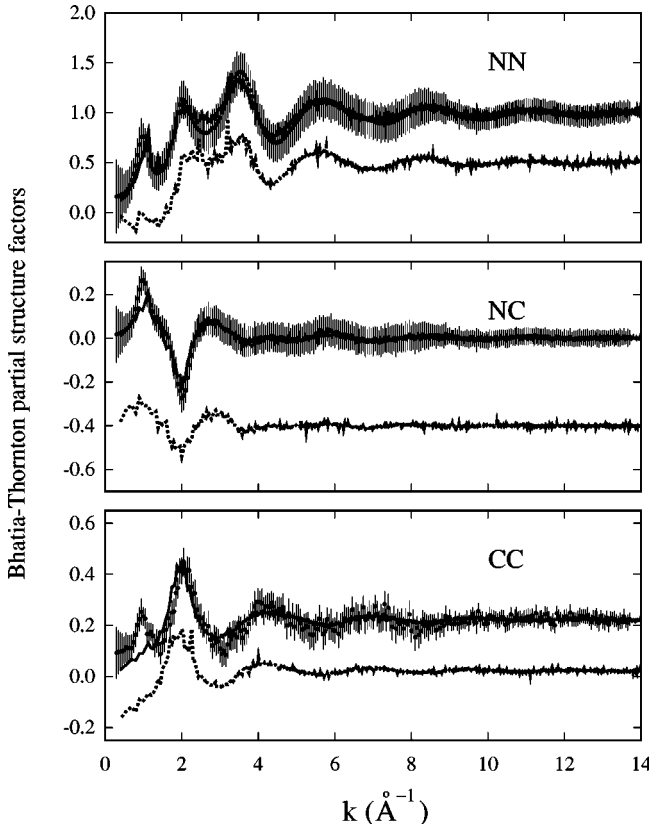


FIG. 2. The Bhatia-Thornton partial structure factors (Ref. 20) for liquid  $\text{GeSe}_2$ : GGA calculations (solid line), LDA calculations (dotted line), and experiment (dots with error bars) (Ref. 37)  $S_{NN}^{LDA}(k)$ ,  $S_{NC}^{LDA}(k)$ , and  $S_{CC}^{LDA}(k)$  have been shifted down by 0.5, 0.4, and 0.2, respectively.

experiment is found for the Se-Se structure factor  $S_{SeSe}^{GGA}(k)$ . In particular, this partial structure factor reproduces well the small signature found at the position of the FSDP, the main peak, and the adjacent minimum.

In Fig. 2, we further analyze the comparison between theory and experiment by considering the Bhatia-Thornton<sup>20</sup> partial structure factors  $S_{NN}(k)$  (number-number),  $S_{NC}(k)$  (number-concentration), and  $S_{CC}(k)$  (concentration-concentration). These can be obtained by linear combinations of the FZ structure factors.<sup>36</sup> In terms of the Bhatia-Thornton structure factors, the total neutron structure factor  $S_T(k)$  reads

$$S_T(k) = S_{NN}(k) + A[S_{CC}(k)/c_{Ge}c_{Se} - 1] + BS_{NC}(k), \quad (1)$$

where  $A = c_{Ge}c_{Se}\Delta b^2/\langle b \rangle^2$ ,  $B = 2\Delta b/\langle b \rangle$ ,  $\Delta b = b_{Ge} - b_{Se}$ , and  $\langle b \rangle = c_{Ge}b_{Ge} + c_{Se}b_{Se}$ ,  $c_\alpha$  and  $b_\alpha$  denoting the atomic fraction and the coherent scattering length of the chemical species  $\alpha$  ( $b_{Ge} = 8.185$  fm,  $b_{Se} = 7.97$  fm).<sup>19</sup> This leads to coefficients  $A$  and  $B$  equal to  $1.6 \times 10^{-4}$  and 0.053, respectively. Due to the close values of the scattering lengths of Ge and Se and the limited range of variation of  $S_{NC}(k)$  and  $S_{CC}(k)$  [ $|S_{NC}(k)| < 0.2$ ,  $S_{CC}(k) < 0.5$ ; see Fig. 2],  $S_{NN}(k)$  turns out to be a very good approximation for  $S_T(k)$ , i.e.,  $|S_T(k) - S_{NN}(k)| < 0.015$ . The significance of the

concentration-concentration structure factor  $S_{CC}(k)$  can be appreciated by considering the relation

$$S_{CC}(k) = c_{Ge}c_{Se}(1 + c_{Ge}c_{Se}\{[S_{GeGe}(k) - S_{GeSe}(k)] + [S_{SeSe}(k) - S_{GeSe}(k)]\}). \quad (2)$$

This equality shows that a peak at a given wave vector in the  $S_{CC}(k)$  stems from the sensitivity of a given atom (Ge or Se) to the chemical nature of its neighbors on the length scale associated to that specific value of  $k$ . On the contrary, the absence of a peak corresponds to an equivalent tendency to homo- or heteropolar neighbors.

Consistently as found for the total structure factor, our calculated  $S_{NN}^{GGA}(k)$  lies almost entirely within the error bars of the measured  $S_{NN}^{expt}(k)$ , the only notable difference concerning the position of the FSDP, as mentioned above. Also the number-concentration structure factor  $S_{NC}^{expt}(k)$  is well reproduced by the theoretical  $S_{NC}^{GGA}(k)$ , with small differences confined to the FSDP region. The theoretical  $S_{CC}^{GGA}(k)$  agrees closely with the concentration-concentration structure factor  $S_{CC}^{expt}(k)$  for  $k > 1.5 \text{ \AA}^{-1}$ . However, the very prominent FSDP observed experimentally is absent in the theoretical  $S_{CC}^{GGA}(k)$ .

Overall, the comparison between experimental and theoretical partial structure factors is very good for  $k$  values characteristic of short-range properties ( $k > 2 \text{ \AA}^{-1}$ ). However, despite the good agreement in the total structure factor,<sup>21</sup> the distribution of the FSDP weights in the partial structure factors is found to be different in theory and experiment. In the FZ scheme, this difference is manifest in the Ge-Ge and, to a lesser extent, in the Ge-Se partial structure factors. While these discrepancies compensate in the total structure factor, they concur to give an important deviation with respect to experiment at the FSDP position of the BT concentration-concentration structure factor, according to Eq. (2).

In the case of the LDA, the agreement with experiments for the partial structure factors is only qualitative over the entire  $k$  range (Fig. 1). The most remarkable difference with respect to the GGA results is the absence of a FSDP in the  $S_{GeGe}^{LDA}(k)$  structure factor. Overall, the  $S_{GeGe}^{LDA}(k)$  is less structured than its GGA counterpart, showing shallower maxima and minima and a very flat trend for  $k > 3 \text{ \AA}^{-1}$ . A similar pattern is observed for  $S_{GeSe}^{LDA}(k)$  and  $S_{SeSe}^{LDA}(k)$ , where heights and depths of the features are severely underestimated.

Figure 2 also gives the BT structure factors calculated in the LDA. The theoretical  $S_{NN}^{LDA}(k)$  does not show a FSDP, consistent with the total structure factor,<sup>22</sup> of which it gives an accurate representation [see Eq. (1)]. At higher  $k$  values,  $S_{NN}^{LDA}(k)$  yields flatter peaks in between  $2 \text{ \AA}^{-1}$  and  $4 \text{ \AA}^{-1}$  and, for  $k > 4 \text{ \AA}^{-1}$ , less pronounced oscillations than  $S_{NN}^{GGA}(k)$ , in marked contrast with the corresponding experimental structure factor. Similarly, the LDA structure factors  $S_{NC}^{LDA}(k)$  and  $S_{CC}^{LDA}(k)$  are found to be less structured than in the GGA. The sizable shoulder exhibited in  $S_{NN}^{LDA}(k)$ , close to the FSDP location at  $k < 0.9 \text{ \AA}^{-1}$ , should not be taken as an indication of the presence of a FSDP. Indeed, the values of  $S_{NN}^{LDA}(k)$  assumed in this region are consistent with the total structure factor measured by neutron diffraction for liq-

liquid GeSe<sub>2</sub> at high temperatures,<sup>39</sup> where the FSDP vanishes. Recent first-principles molecular dynamics simulations, which successfully modeled this behavior, showed a concomitant collapse of intermediate-range order.<sup>40</sup>

Recently, Cobb and Drabold modeled liquid GeSe<sub>2</sub> within a non-self-consistent electronic structure scheme based on the LDA and on the use of a minimal basis set.<sup>41</sup> Overall, their results are consistent with experiment. However, a FSDP arises in the total structure factor, at variance with our fully self-consistent LDA results. Given the relation between ionicity and the FSDP,<sup>22</sup> this suggests that the approximations inherent in the calculations of Ref. 41 artificially enhance the ionic character of the bonding compared to a converged LDA calculation.

In summary, the LDA appears inadequate to account for short- and intermediate-range order in liquid GeSe<sub>2</sub>. The GGA improves upon the LDA description and brings the calculated structure factors into much better agreement with the experimental ones. However, small differences remain between experiment and theory when one focuses on the height of the FSDP in the partial structure factors. Most striking is the absence of the FSDP in the  $S_{CC}^{GGA}(k)$ , which is closely related to an underestimation of the height of the FSDP in the Ge-Ge structure factor.

### B. Pair correlation functions

Partial pair correlation functions  $g_{\alpha\beta}(r)$  and their experimental counterparts<sup>19,38</sup> are shown in Fig. 3. Peak positions and number of neighbors within given integration ranges are displayed in Table II. A first maximum indicative of homopolar bonds is clearly distinguishable in the experimental  $g_{GeGe}^{expt}(r)$ , followed by a main peak and a deep minimum, showing distinct shells of neighbors. This trend is not accurately reproduced by the theoretical  $g_{GeGe}^{GGA}(r)$ , which is characterized by the absence of a clear first maximum, a larger distance for homopolar bonds, a broader main peak, and a much less pronounced first minimum. By consequence, the theoretical Ge-Ge coordination number  $n_{GeGe}$  calculated over distances corresponding to the first experimental peak ( $0 < r < 2.6$  Å) underestimates the experimental value. The Ge-Se pair correlation function  $g_{GeSe}^{expt}(r)$  is characterized by a prominent main peak and a deep minimum. This behavior is well reproduced in the theoretical  $g_{GeSe}^{GGA}(r)$ , though the maximum and the minimum are found to be less pronounced. At higher distances, the theoretical  $g_{GeSe}^{GGA}(r)$  shows less structure than the experimental curve, with a flat second maximum at  $r = 5.5$  Å. The first-neighbor Ge-Se coordination numbers  $n_{GeSe}$  derived from the experiment and from the simulation compare satisfactorily. In the case of Se-Se correlations, the theoretical  $g_{SeSe}^{GGA}(r)$  follows closely the experimental  $g_{SeSe}^{expt}(r)$  for  $r > 3$  Å. Although the first peak is sharper than in experiment, the  $g_{SeSe}^{GGA}(r)$  yields an accurate value for the first-neighbor coordination number  $n_{SeSe}$ . Considering the results obtained in the LDA, we observe the following. On the one hand, the overall shape of the three LDA partial correlation functions is remarkably similar to the GGA ones. On the other hand, the LDA curves show a

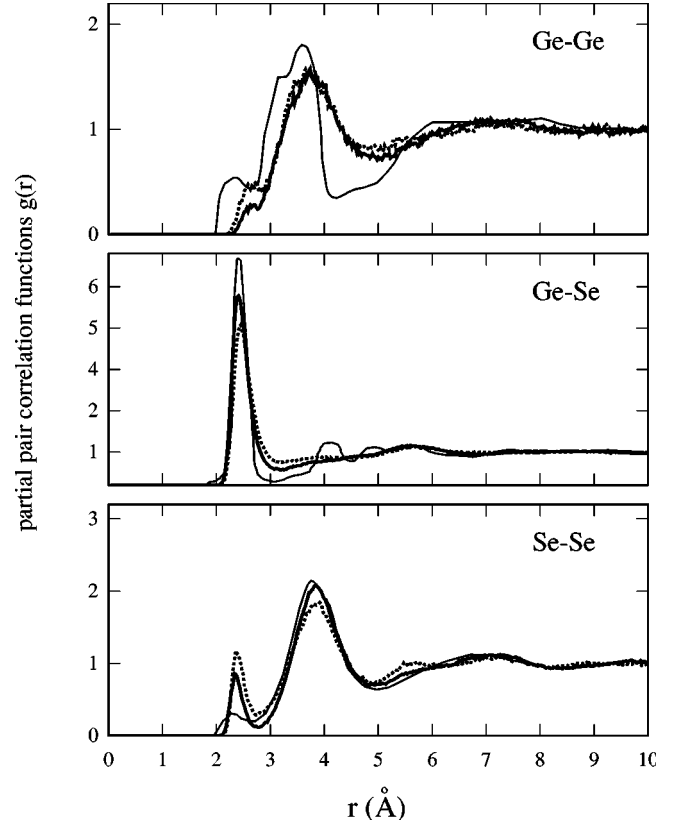


FIG. 3. Partial pair correlation functions for liquid GeSe<sub>2</sub>: GGA calculations (thick line), LDA calculations (dotted line), and experimental data (solid line) (Refs. 19 and 38).

higher number of homopolar neighbors and are generally less structured than in the GGA.

We obtain partial ( $n_{Ge}$ ,  $n_{Se}$ ) and average ( $n$ ) coordination numbers from the first-neighbor coordination numbers

TABLE II. First (FPP) and second (SPP) peak positions in experimental (Refs. 19 and 38) and theoretical  $g_{\alpha\beta}(r)$ . The integration ranges corresponding to the coordination numbers  $n_{\alpha\beta}$  and  $n'_{\alpha\beta}$  are 0–2.6 Å, 2.6–4.2 Å for  $g_{GeGe}(r)$ , 0–3.1 Å, 3.1–4.5 Å for  $g_{GeSe}(r)$ , and 0–2.7 Å, 2.7–4.8 Å for  $g_{SeSe}(r)$ . Error bars are the standard deviations from the mean for subaverages of 2 ps (GGA) and 1 ps (LDA).

$g_{\alpha\beta}(r)$	FPP (Å)	$n_{\alpha\beta}$	SPP (Å)	$n'_{\alpha\beta}$
$g_{GeGe}^{LDA}(r)$	$2.7 \pm 0.1$	$0.08 \pm 0.01$	$3.65 \pm 0.10$	$2.89 \pm 0.06$
$g_{GeGe}^{GGA}(r)$	$2.7 \pm 0.1$	$0.04 \pm 0.01$	$3.74 \pm 0.05$	$2.74 \pm 0.06$
$g_{GeGe}^{expt}(r)$	$2.33 \pm 0.03$	$0.25 \pm 0.10$	$3.59 \pm 0.02$	$2.9 \pm 0.3$
$g_{GeSe}^{LDA}(r)$	$2.45 \pm 0.10$	$3.68 \pm 0.01$	$5.70 \pm 0.02$	$4.32 \pm 0.06$
$g_{GeSe}^{GGA}(r)$	$2.41 \pm 0.10$	$3.76 \pm 0.01$	$5.60 \pm 0.01$	$3.72 \pm 0.03$
$g_{GeSe}^{expt}(r)$	$2.42 \pm 0.02$	$3.5 \pm 0.2$	$4.15 \pm 0.10$	$4.0 \pm 0.3$
$g_{SeSe}^{LDA}(r)$	$2.36 \pm 0.07$	$0.56 \pm 0.02$	$3.82 \pm 0.05$	$8.9 \pm 0.06$
$g_{SeSe}^{GGA}(r)$	$2.34 \pm 0.02$	$0.37 \pm 0.01$	$3.84 \pm 0.02$	$9.28 \pm 0.04$
$g_{SeSe}^{expt}(r)$	$2.30 \pm 0.02$	$0.23 \pm 0.05$	$3.75 \pm 0.02$	$9.6 \pm 0.3$

TABLE III. Experimental and theoretical values for the partial coordination numbers  $n_{Ge}$  and  $n_{Se}$  and the average coordination number  $n$  of liquid  $GeSe_2$  at  $T=1040$  K. The coordination numbers  $n_{Ge}$  and  $n_{Se}$  are given by  $n_{GeGe} + n_{GeSe}$ , and  $n_{SeSe} + n_{SeGe}$ , respectively (see the values reported in Table II for  $n_{GeGe}$ ,  $n_{GeSe}$ , and  $n_{SeSe}$ , where  $n_{GeSe}=2n_{SeGe}$ ). The average coordination number  $n$  is equal to  $c_{Ge}(n_{GeGe} + n_{GeSe}) + c_{Se}(n_{SeSe} + n_{SeGe})$ . Error bars are the standard deviations of the mean for subaverages of 2 ps.

	$n_{Ge}$	$n_{Se}$	$n$
LDA	$3.76 \pm 0.02$	$2.40 \pm 0.02$	$2.85 \pm 0.02$
GGA	$3.80 \pm 0.02$	$2.25 \pm 0.02$	$2.77 \pm 0.02$
Ref. 38	$3.75 \pm 0.3$	$1.98 \pm 0.15$	$2.57 \pm 0.20$

$n_{GeGe}$ ,  $n_{GeSe}$ , and  $n_{SeSe}$  given in Table II. The resulting theoretical values are compared to experimental data in Table III. Overall, the GGA partial and average coordination numbers reproduce well the experimental results. The coordination numbers  $n_{Se}$  and  $n$  obtained in the LDA compare less favorably: this discrepancy can be traced back to  $n_{SeSe}$ . We note that the good agreement between theory and experiment found for  $n_{Ge}$  is somewhat fortuitous, because it results from the compensation of the calculated  $n_{GeGe}$  and  $n_{GeSe}$ , particularly for the LDA.

Our results in real space confirm that the GGA provides a better description of liquid  $GeSe_2$  than the LDA. The theoretical pair correlation functions  $g_{GeSe}^{GGA}(r)$  and  $g_{SeSe}^{GGA}(r)$  are found to be consistent with the corresponding experimental ones.<sup>19</sup> However, our model yields a broader distribution of Ge—Ge bond lengths, which on average are longer by as much as 15% with respect to experimental values (see Table II). Longer interatomic Ge—Ge distances and less structured Ge-Ge pair correlation functions were recently also obtained for liquid  $GeSe$  within the same first-principles framework used here.<sup>42</sup> We note that such longer Ge—Ge bond lengths are characteristic of the metallic liquid Ge. For this system, first-principles calculations correctly reproduce the experimental bond lengths (theory,<sup>43,44</sup> 2.63–2.75 Å; experiment,<sup>45,46</sup> 2.66–2.75 Å). This suggests that the GGA overestimates the metallic character in liquid  $GeSe_2$  and  $GeSe$ .

Throughout our work, we assumed that the composition of liquid  $GeSe_2$  is homogeneous on nanoscale distances. However, it should be noted that this assumption has recently been challenged by Boolchand and Bresser.<sup>13</sup> By associating the connectivity of the network to the dependence of the glass transition temperature on  $x$  in  $Ge_xSe_{1-x}$  binary glasses, these authors interpreted the observed trends in terms of evidence for the growth of a minority Ge-rich  $Ge_2(Se_{1/2})_6$  phase, a phase separated on the nanoscale from the majority Se-rich  $Ge(Se_{1/2})_4$  phase.<sup>13</sup> Such a model is consistent with the observation of homopolar bonds in Mössbauer,<sup>7,8,13</sup> Raman,<sup>6,9,10,13</sup> and diffraction measurements.<sup>12,19</sup> However, it is, at present, not yet clear whether this interpretation might also offer a natural explanation for structural properties involving intermediate-range order, such as the observation of

TABLE IV. Average number  $n_\alpha(l)$  (boldface characters, expressed as a percentage) of atoms of species  $\alpha$  ( $\alpha=Ge, Se$ )  $l$ -fold coordinated at a distance of 3 Å. For each value of  $n_\alpha(l)$ , we give the identity and the number of the Ge and Se neighbors. Note that 0.45% of the Ge atoms have a coordination  $l=6$  (not reported in the table). In the lower part of the table, we also give the average number of dimers, trimers, tetramers, and pentamers. Atoms are considered bonded when their separation is smaller than 3 Å. Statistical errors do not exceed 2%.

		$l=1$	<b>0.20</b>	$l=2$	<b>5.26</b>	
<b>Ge</b>		Ge	-	Ge <sub>2</sub>	-	
		Se	0.20	GeSe	0.09	
				Se <sub>2</sub>	5.17	
	$l=3$	<b>22.37</b>	$l=4$	<b>60.88</b>	$l=5$	<b>10.83</b>
	Ge <sub>3</sub>	-	Ge <sub>4</sub>	-	Ge <sub>5</sub>	-
	Ge <sub>2</sub> Se	-	Ge <sub>3</sub> Se	-	Ge <sub>4</sub> Se	-
	GeSe <sub>2</sub>	2.61	Ge <sub>2</sub> Se <sub>2</sub>	0.10	Ge <sub>3</sub> Se <sub>2</sub>	-
	Se <sub>3</sub>	19.76	GeSe <sub>3</sub>	6.95	Ge <sub>2</sub> Se <sub>3</sub>	0.36
			Se <sub>4</sub>	53.83	GeSe <sub>4</sub>	5.89
					Se <sub>5</sub>	4.58
<b>Se</b>		$l=1$	<b>2.28</b>	$l=2$	<b>70.30</b>	
		Se	0.55	Se <sub>2</sub>	2.83	
		Ge	1.73	SeGe	21.90	
				Ge <sub>2</sub>	45.57	
	$l=3$	<b>25.27</b>	$l=4$	<b>2.13</b>	$l=5$	<b>0.04</b>
	Se <sub>3</sub>	0.32	Se <sub>4</sub>	0.01	Se <sub>5</sub>	-
	Se <sub>2</sub> Ge	3.25	Se <sub>3</sub> Ge	0.09	Se <sub>4</sub> Ge	-
	SeGe <sub>2</sub>	8.58	Se <sub>2</sub> Ge <sub>2</sub>	0.59	Se <sub>3</sub> Ge <sub>2</sub>	0.01
	Ge <sub>3</sub>	13.12	SeGe <sub>3</sub>	1.04	Se <sub>2</sub> Ge <sub>3</sub>	0.02
			Ge <sub>4</sub>	0.40	SeGe <sub>4</sub>	0.01
				Ge <sub>5</sub>	-	
		dimers	trimers	tetramers	pentamers	
<b>Ge</b>		2.9	0.3			
<b>Se</b>		8.9	3.1	0.9	0.2	

a FSDP in the concentration-concentration structure factor<sup>19,37</sup> or the detailed shape of the Ge-Ge partial correlation function.<sup>19,38</sup>

#### IV. STRUCTURAL PROPERTIES

All the results presented hereafter refer to the calculations performed within the GGA scheme.

##### A. Coordination numbers and bond angle distributions

We defined  $n_\alpha(l)$  as the average number of atoms of species  $\alpha$   $l$ -fold coordinated (Table IV), where  $\alpha$  are Ge or Se atoms. We here used a cutoff distance of 3 Å, which corresponds to the first minimum in the Ge—Se pair correlation function and describes well the first shell of neighbors also

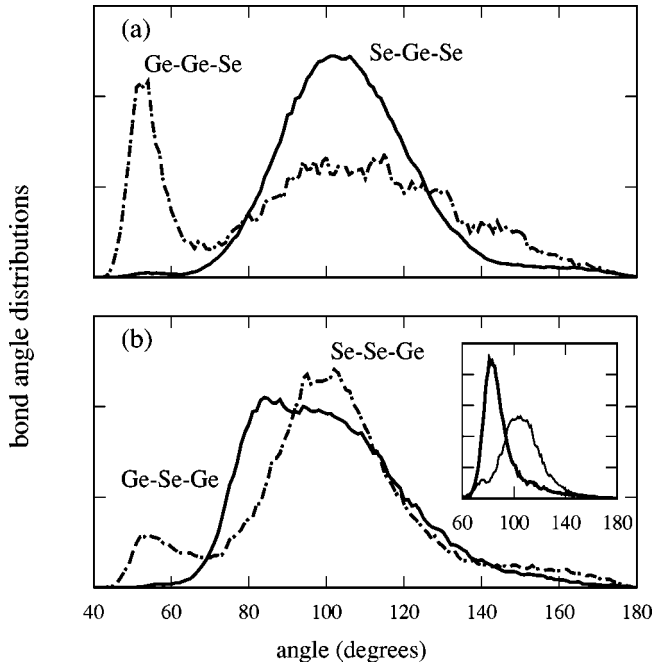


FIG. 4. Bond-angle distributions Se—Ge—Se (top, solid line), Ge—Ge—Se (top, dashed-dotted line), Ge—Se—Ge (bottom, solid line), and Se—Se—Ge (bottom, dash-dotted line). Inset: Ge—Se—Ge bond angle distributions obtained by considering separately Ge atoms belonging to edge-sharing (thick) and corner-sharing (thin) configurations.

for Ge—Ge and Se—Se correlations. In Table IV, we also report the population of homopolar  $n$ -mers of Ge and Se atoms.

The percentage of fourfold-coordinated Ge atoms is close to 61%. Among the Ge atoms,  $\sim 54\%$  form  $\text{GeSe}_4$  tetrahedra and  $\sim 7\%$  are found in Ge— $\text{GeSe}_3$  units with one Ge—Ge homopolar bond. Threefold-coordinated Ge atoms occur in non-negligible amounts (22.4%), yielding Ge— $\text{Se}_3$  (19.8%) and Ge— $\text{GeSe}_2$  (2.6%) units. Fivefold-coordinated Ge atoms (10.8%) are also present, distributed in close proportions among Ge— $\text{GeSe}_4$  and Ge— $\text{Se}_5$  units. In the case of Ge, the percentage of atoms forming homopolar bonds (16.5%) is in good agreement with experimental estimates for amorphous  $\text{GeSe}_2$ .<sup>8,12</sup>

The Se atoms show a pronounced preference for twofold bonding (70.3%), under the form of Se— $\text{SeGe}$  (21.9%) and Se— $\text{Ge}_2$  (45.6%) units. As much as 25% of the Se atoms are threefold coordinated, as shown by the occurrence of Se— $\text{SeGe}_2$  (8.6%) and Se— $\text{Ge}_3$  (13.1%) units. Homopolar bonding involves as much as 32% of the Se atoms, which form on average  $\sim 9$  dimers and  $\sim 3$  trimers in our model.

Further information on the network topology can be gained via the distribution of the Se—Ge—Se, Ge—Ge—Se, Ge—Se—Ge, and Se—Se—Ge bond angles, which are shown in Fig. 4. These distributions have been calculated by including neighbors separated by less than  $3 \text{ \AA}$ . The Se—Ge—Se bond distribution is highly symmetric with a maximum at  $103^\circ$  and an average angle equal to  $106^\circ$ . Despite the occurrence of a variety of bonding configurations, these values lie close to the tetrahedral angle.

TABLE V. Distribution of rings in liquid  $\text{GeSe}_2$ . NR is the total number of rings of a given size.  $\text{NR}(n)$  is the number of rings having  $n$  Ge atoms ( $n=1, \dots, 7$  Ge). We also give the average number of Ge atoms ( $N_{\text{Ge}}$ ) found in a ring of a given size. Statistical errors do not exceed 5%.

Ring size	3	4	5	6	7	8	9	10	11	12
NR	5.1	11.6	6.6	5.4	2.6	2.9	1.3	2.6	2.3	3.1
NR(1 Ge)	2.2	0.4								
NR(2 Ge)	2.9	11.1	4.7	0.6	0.2					
NR(3 Ge)		0.1	1.9	4.8	2.0	0.8	0.1	0.1		
NR(4 Ge)					0.4	2.1	0.9	0.5	0.4	0.1
NR(5 Ge)							0.3	2.0	1.6	0.9
NR(6 Ge)									0.3	2.0
NR(7 Ge)										0.1
$N_{\text{Ge}}$	7.7	18.1	14.5	14.5	7.7	10.3	5.1	11.7	11.0	16.7

The Ge—Ge—Se distribution shows two components. A prominent peak is observed for angles close to  $60^\circ$ , indicating the presence of threefold rings. The second component corresponds to a broad distribution at higher angles in the interval  $80^\circ$ – $120^\circ$ . Because this component is found to be broader than the Se—Ge—Se bond distribution, we infer that the occurrence of a Ge—Ge bond as part of Ge-centered motifs increases the angular flexibility of these subunits.

The Ge—Se—Ge bond distribution is characterized by a flat maximum extending from  $80^\circ$  to  $100^\circ$ , which can be interpreted in terms of two type of configurations.<sup>16</sup> The shoulder on the left side of this interval arises from edge-sharing tetrahedra, i.e., Ge-centered subunits which have in common two Se atoms. The remaining part of the main peak then results from corner-sharing tetrahedra, which share only a single Se atom. Such a decomposition is confirmed by the plot shown in the inset of Fig. 4(b), where the Ge—Se—Ge distributions corresponding to edge- and corner-sharing tetrahedra are shown separately. The Se—Se—Ge bond distribution shows two peaks. One of the peaks is centered at angles in between  $50^\circ$  and  $60^\circ$ , and results from the occurrence of Se—Se bonds in triangular motifs. The other peak occurs at  $\sim 100^\circ$ , indicating corner-sharing-like rather than edge-sharing-like connections. We infer that Se—Se bonds are unlikely to be found in fourfold rings.

### B. Ring statistics

Several molecular dynamics studies have determined rings statistics in amorphous and liquid  $\text{GeSe}_2$ .<sup>15,41</sup> Our distribution of rings is given in Table V. We used the counting algorithm based on the shortest-path criterion proposed by Franzblau.<sup>47,48</sup> Fourfold rings are the most likely to form, but they coexist with a substantial amount of threefold, fivefold, and sixfold rings. We note that for a given even-membered ring, the configuration with an equal number of Ge and Se atoms is always favored. In the case of odd-membered rings, a clear preference for Se-rich rings is observed, consistently with the occurrence of a large number of Se—Se homopolar bonds.

Since some of the atoms could belong to more than one ring of a given size, we separately provide in Table V average numbers of Ge atoms as distributed among the different rings. For instance, we found that 45% and 36% of the Ge atoms are found in fourfold and fivefold rings, respectively. The percentage of Ge atoms found in edge sharing configurations is in very good agreement with the experimental estimate ( $\sim 50\%$ ).<sup>19</sup> The Ge atoms can further be subdivided in classes of  $\text{Ge}(n)$  atoms which differ by the number  $n$  of fourfold rings to which they belong. For instance, the  $\text{Ge}(2)$  atoms characterize the bonding in crystalline  $\text{SiSe}_2$ ,<sup>49</sup> where all the tetrahedra are edge-sharing. Another example is the high-temperature crystalline polymorph of  $\text{GeSe}_2$  which features an equal number of corner-sharing  $\text{Ge}(0)$  and edge sharing  $\text{Ge}(1)$  sites.<sup>50</sup> From this subdivision we deduce that, considering all Ge atoms, 55% do not belong to fourfold rings, 36% belong to a single fourfold ring, and 9% belong to two fourfold rings.

### C. Real-space correlations and the FSDP

We here focus on the range of real-space correlations which are responsible for the appearance of the FSDP. For a given partial pair correlation function  $g_{\alpha\beta}(r)$ , this range can be determined by truncating  $g_{\alpha\beta}(r)$  at decreasing distances  $r_c$  and by monitoring the behavior of the corresponding Fourier-transformed structure factor  $S_{\alpha\beta}(k)$ . These two quantities are related as follows:

$$S_{\alpha\beta}(k) = 1 + 4\pi\rho \int_0^{r_c} r^2 [g_{\alpha\beta}(r) - 1] \frac{\sin kr}{kr} dr, \quad (3)$$

where  $\rho$  is the atomic number density. Correlations exceeding the size of the supercell (cubic cell of side  $L = 15.7 \text{ \AA}$ ) are obtained by taking into account the periodic character of our model system. In practice, we replicate our periodic cell by one unit in three directions up to a system containing 3240 atoms (27 times more atoms than the original one). This size allows us to calculate the pair correlation functions up to distances as large  $r_{max} = 33 \text{ \AA}$ . We first verified that the structure factor  $S_{GeGe}(k)$  obtained by using Eq. (3) with  $r_c = r_{max}$  is very close to the result of the direct calculation in  $k$  space shown in Fig. 1. This comparison is shown in Fig. 5(a). Upon reducing the integration range a sizable reduction of the FSDP height begins to manifest. However, a well-defined peak still persists at the FSDP location when  $r_c$  extends up to  $10.5 \text{ \AA}$  [Fig. 5(b)]. This  $r_c$  is smaller than  $\sqrt{2}L/2$ , a value for which reliable statistics can be gathered for distances between independent atoms in a cubic supercell.<sup>51</sup> For shorter truncation radii [ $r_c = 6 \text{ \AA}$ , Fig. 5(c)], only a residual bump remains at the FSDP location, and, for the even shorter  $r_c = 5 \text{ \AA}$  [Fig. 5(d)], any residual feature disappears. In analogy with a similar study performed on a classical molecular dynamics model of liquid  $\text{GeSe}_2$ ,<sup>16</sup> we conclude that the FSDP in the  $S_{GeGe}(k)$  structure factor is mainly due to correlations beyond  $5 \text{ \AA}$ .

We carried out the same analysis as a function of  $r_c$  for the total neutron structure factor  $S_T(k)$ . The results are given in Fig. 6. Direct and Fourier-transformed  $S_T(k)$  are in very

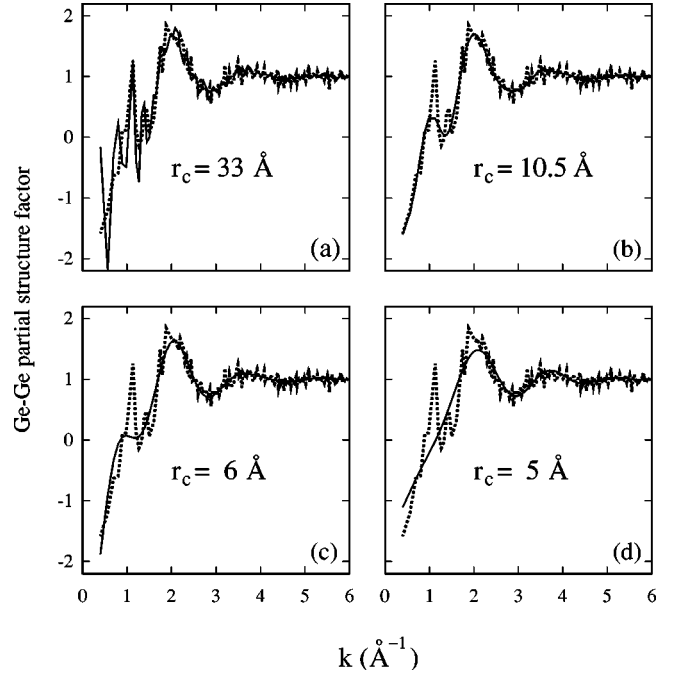


FIG. 5. Ge—Ge partial structure factors for liquid  $\text{GeSe}_2$  (solid lines) obtained by Fourier integration of the calculated partial pair correlation function  $g_{GeGe}(r)$  within given integration ranges  $0 - r_c$ : (a)  $r_c = 33 \text{ \AA}$ , (b)  $r_c = 10.5 \text{ \AA}$ , (c)  $r_c = 6 \text{ \AA}$ , and (d)  $r_c = 5 \text{ \AA}$ . The dotted line corresponds to the partial structure factor directly calculated in  $k$  space.

good agreement over the entire  $k$  range when  $r_c = r_{max}$ . The Fourier-transformed structure factor is more noisy than the direct one in the low- $k$  region. However, the FSDP is well reproduced [Fig. 6(a)]. The FSDP remains clearly discernible for  $r_c = 10.5 \text{ \AA}$  [Fig. 6(b)], and, although less prominent, for  $r_c = 6 \text{ \AA}$  [Fig. 6(c)]. Further reduction of the truncation range to  $r_c = 5 \text{ \AA}$  [Fig. 6(d)] drastically flattens the feature at  $k = 1 \text{ \AA}^{-1}$ , which turns into a shoulder located in between  $1 \text{ \AA}^{-1}$  and  $1.5 \text{ \AA}^{-1}$ . The similar behavior observed in Fig. 5 and Fig. 6 is consistent with the fact that the FSDP is mostly due to Ge—Ge correlations. However, the persistence of a shoulder in  $S_T(k)$  in Fig. 6(d), which is not observed in the corresponding  $S_{GeGe}(k)$  [Fig. 5(d)], proves that the FSDP also carries contributions from Ge—Se and, to a much smaller extent, Se—Se correlations (Fig. 1).

We here showed that, for finite  $L$ , the direct calculation of the FSDP in reciprocal space is different than obtained using the Fourier transform of the pair correlation function limited to distances between independent atoms in the supercell [Fig. 5(b)]. For simulations with sufficiently large supercells ( $L \rightarrow \infty$ ) the two calculation schemes are equivalent. However, for finite  $L$ , the above results show that the convergence of the FSDP height with  $L$  can be different. In the absence of a complete investigation as a function of  $L$ , which is beyond the scope of the present study, it is difficult to assess which of the two schemes shows a faster convergence. However, it should be emphasized that direct calculations in reciprocal space often produced structure factors in very good agreement with experiment.<sup>21,51–60</sup>

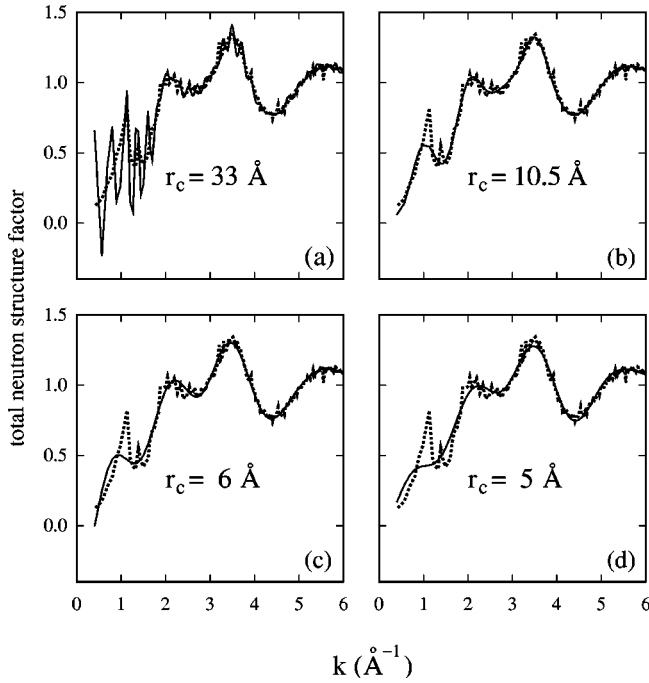


FIG. 6. Total neutron structure factor for liquid  $\text{GeSe}_2$  (solid lines) obtained by Fourier integration of the calculated partial pair correlation functions  $g_{\text{GeGe}}(r)$ ,  $g_{\text{GeSe}}(r)$ , and  $g_{\text{SeSe}}(r)$  within given integration ranges  $0-r_c$ : (a)  $r_c=33$  Å, (b)  $r_c=10.5$  Å, (c)  $r_c=6$  Å, and (d)  $r_c=5$  Å. The dotted line corresponds to the total neutron structure factor directly calculated in  $k$  space.

## V. DYNAMICAL PROPERTIES

The calculated statistical average of the time-dependent quantity

$$D_\alpha(t) = \frac{1}{6tN_\alpha} \left\langle \sum_{i=1}^{N_\alpha} |\mathbf{r}_{i\alpha}(t) - \mathbf{r}_{i\alpha}(0)|^2 \right\rangle \quad (4)$$

for both species  $\alpha$ , Ge and Se, is shown in Fig. 7. In Eq. (4),  $\mathbf{r}_{i\alpha}(t)$  is the coordinate of the  $i$ th particle at time  $t$  and  $N_\alpha$  is the number of particles of the species  $\alpha$ . Plateau values of  $D_\alpha(t)$  are attained after 5–6 ps and yield diffusion coefficients of  $D_{\text{Ge}} = (2.2 \pm 0.2) \times 10^{-5} \text{ cm}^2/\text{s}$  and  $D_{\text{Se}} = (2.2 \pm 0.2) \times 10^{-5} \text{ cm}^2/\text{s}$ . Error bars are those of  $D_\alpha(t)$  for  $t = 4$  ps and have been attributed by taking subaverages on trajectories of 5 ps each. Equal diffusivity for the two species in liquid  $\text{GeSe}_2$  contrasts the results obtained for liquid  $\text{GeSe}$  at about the same temperature. For this system, diffusion coefficients of  $D_{\text{Ge}} = (2.8 \pm 0.3) \times 10^{-5} \text{ cm}^2/\text{s}$  and  $D_{\text{Se}} = (2.0 \pm 0.3) \times 10^{-5} \text{ cm}^2/\text{s}$  were obtained, which indicate that in  $\text{GeSe}$  the Ge atoms are more mobile than the Se ones.<sup>42</sup> This behavior can be rationalized by noting that, in the nonstoichiometric  $\text{GeSe}$ , the increase of homopolar Ge—Ge bonds weakens the network allowing the Ge atoms to migrate more easily.<sup>42</sup>

In the inset of Fig. 7, we show the average bond lifetimes of Ge—Ge, Se—Se, and Ge—Se pairs, as calculated for varying cutoff distances  $d_c$ , in the range of first-neighbor distances. In principle, one could simply define this quantity as the average time during which a bond is shorter than a

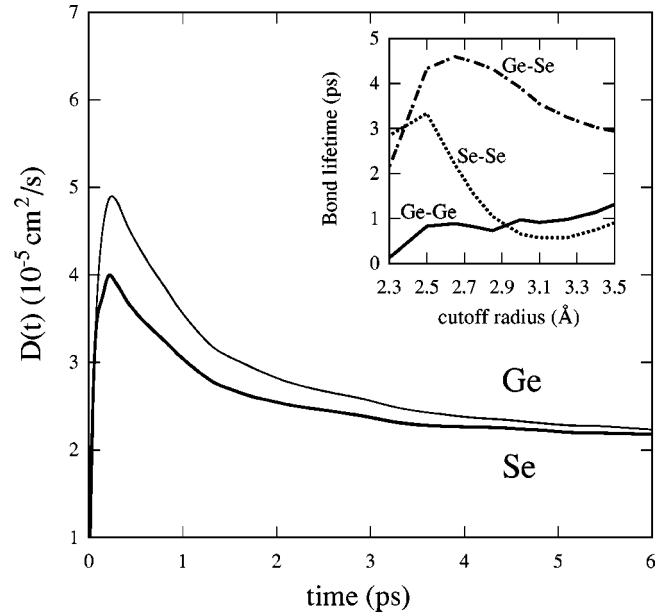


FIG. 7. Diffusion coefficients for Ge and Se atoms in liquid  $\text{GeSe}_2$ . Inset: bond lifetimes for Ge—Ge, Se—Se, and Ge—Se pairs of atoms as a function of cutoff radius.

given  $d_c$ . However, in such a procedure, a bond would be considered broken for any temporary fluctuation of the interatomic distance beyond the cutoff radius  $d_c$ . Therefore, we here adopted a different procedure in which a bond is considered broken when its interatomic distance remains larger than  $d_c$  for a time period longer than a given residence time  $t_{\text{res}}$ .<sup>61</sup> We took a value of 0.7 ps for  $t_{\text{res}}$  using a typical frequency in the vibrational spectrum of amorphous  $\text{GeSe}_2$  ( $\nu=40$  meV).<sup>62</sup> Interestingly, this choice coincides with the approximate width of the first-neighbor peak in the pair correlation functions (1 Å) and the value of the diffusion coefficient.

The calculated bond lifetimes of Ge—Ge pairs give values of about 1 ps, showing only a small increase for increasing bond length  $d_c$ . This implies that the Ge—Ge bonds do not show any proclivity for a specific bond length in the investigated range of  $d_c$ . By contrast, the Ge—Se lifetimes are much longer, ranging between 3 and 5 ps. The longest lifetime is found for a value of  $d_c$  which corresponds well to the position of the main peak in the Ge—Se pair correlation function. Such a trend is consistent with the predominant occurrence of  $\text{GeSe}_4$  tetrahedra.<sup>22</sup> The Se—Se bonds are also long living for cutoffs  $d_c$  close to their typical bond lengths ( $\sim 2.5$  Å). The rapid decrease of the lifetimes for larger  $d_c$  is indicative of little resistance to bond stretching. Overall, this description shows that the bond lifetimes reflect the behavior of the respective pair correlation functions. These results point out the existence of a correlation between the predominant occurrence of tetrahedra, the establishment of intermediate-range order, and the presence of maxima in the Ge—Se bond lifetime patterns. Indeed, no maxima are found in the bond lifetimes of liquid  $\text{GeSe}$ , where IRO is not observed.<sup>42</sup>

## VI. CONCLUSIONS

Disordered  $\text{GeSe}_2$  systems are interesting examples of random network structures in which the chemical order is broken by the occurrence of homopolar bonds. Indeed, the close electronegativities of Ge and Se give rise to bonding properties in which the ionic and covalent character interplay in a subtle way. For these reasons, liquid and glassy  $\text{GeSe}_2$  have attracted particular attention as prototypes of defective network-forming systems. In particular, the total neutron structure factor shows a distinct first sharp diffraction peak, indicating the occurrence of intermediate-range order. In this work, we addressed the short-range and intermediate-range structure in liquid  $\text{GeSe}_2$  by performing extended molecular dynamics simulations within density functional theory. We adopted a first-principles approach in order to account in an unbiased way for the variety of bonding configurations occurring in this liquid.

In the first part of our work, we performed a close comparison between the results of our simulation and available experimental data. In particular, the comparison comprised the partial structure factors and the partial pair correlations functions, for which detailed experimental results have been obtained.<sup>19</sup> Overall, the agreement with experiment is very good in consideration of the fact that the interatomic interactions in the simulation did not rely on any empirical parameter taken from experiment. In particular, the theory gives good values for the partial and total coordination numbers and for the amount of homopolar bonds. In order to achieve this quality of agreement, it was necessary to resort to a generalized gradient approximation for the exchange and correlation energy. The comparison with experiment shows that the local density approximation results in a structure with an excessive amount of chemical disorder and homopolar bonds. This strongly affects the intermediate-range order as evidenced by the absence of a first sharp diffraction peak in the structure factor calculated in the local density approximation.

Despite the excellent agreement between the measured total neutron structure factor and the one calculated in the generalized gradient approximation, our comparison of partial correlations revealed detailed differences between theory and experiment. The most striking of these differences concerns the first sharp diffraction peak in the concentration-concentration structure factor, which clearly appears in the experiment but is absent in the theory. Our analysis suggests that these limitations are confined to an insufficiently accurate description of Ge—Ge correlations. Indeed, inspection of the Ge—Ge partial structure factor reveals an underestimation of the first sharp diffraction peak. While this underestimation does not affect the total neutron structure factor because of compensation effects related to the other partials structure factors, this discrepancy is magnified in the concentration-concentration structure factor. Moreover, the calculated Ge—Ge pair correlation function is less structured than its experimental counterpart, with first-neighbor distances exceeding the experimental values by about 15%.

The use of the generalized gradient approximation improved upon the local density one, primarily because the

former reproduced more accurately the ionic character in the bonding.<sup>22</sup> This led to a structure with an increased chemical order. It is conceivable that the residual differences between theory and experiment should be attributed to a yet insufficient account of the ionic character in this system. A further increase of the ionicity would naturally lead to an enhancement of the chemical order with a concomitant increase of the height of the Ge—Ge first sharp diffraction peak. This speculation is consistent with our finding of excessively large Ge—Ge bond lengths, which are characteristic of metallic liquid Ge.<sup>43–46</sup>

In the second part of our work, we present an atomistic analysis, which provides insight into the detailed structural properties of the liquid. We found that the Ge-centered tetrahedra are the predominant coordination motifs and coexist with homopolar bonds. Furthermore, a considerable amount of Ge- and Se-centered triads are also observed. These bonding configurations are predicted neither by the continuous random network model<sup>63</sup> nor by its extensions which only include homopolar bonds in addition.<sup>64</sup> Overall, our results show the establishment of a complex network structure, in which the atoms form a variety of bonding configurations differing by both the number and type of nearest neighbors. These properties are further highlighted by the bond angle distributions and ring statistics. The amount of Ge atoms involved in fourfold rings (45%), which occur in edge-sharing tetrahedra but also in other bonding motifs, is consistent with experimental estimates (50%). Among these Ge atoms, a minority (19%) belongs simultaneously to two fourfold rings, in configurations reminiscent of the crystalline structure of  $\text{SiSe}_2$ .<sup>49</sup>

We investigated the intermediate-range order by determining the relevant range of distances responsible for the appearance of the FSDP. To this end, we calculated the structure factors both directly in reciprocal space and through the Fourier transformation of the pair correlation functions. This study revealed that the first sharp diffraction peak results from correlations at distances larger than 5 Å, supporting previous theoretical results obtained with empirical interatomic potentials.<sup>16</sup> We showed that correlations between atoms belonging to different replica in our periodic model contribute to the height of the first sharp diffraction peak. Thus, albeit the use of the periodic approximation, long-range correlations well beyond the size of the supercell are effectively considered in the calculation of the first sharp diffraction peak. This remark suggests that no contradiction exists between the reproducibility of first sharp diffraction peaks calculated for relatively small supercells and the requirement for an appropriate consideration of long-range correlations.

Finally, our investigation concludes by addressing some dynamical properties. In particular, by calculating bond lifetimes, we showed that the most stable bond is the Ge—Se one, consistently with the predominant appearance of  $\text{GeSe}_4$  tetrahedra. While the Se—Se bond lifetimes are almost comparable to the Ge—Se ones, the Ge—Ge ones are considerably shorter, indicating that Ge—Ge homopolar bonds are easily broken.

## ACKNOWLEDGMENTS

We thank P.S. Salmon for useful discussions and for providing experimental data prior to publication. C.M. acknowledges support from the Centre National de la Recherche Scientifique (CNRS) in the framework of the Convention

d'Exchange France-Suisse. A.P. acknowledges support from the Swiss National Science Foundation under Grant No. 620-57850.99. The calculations were performed on the NEC-SX4 of the Swiss Center for Scientific Computing (CSCS) and on the NEC-SX5 of the IDRIS computer center of CNRS (France).

- <sup>1</sup>S. R. Elliott, *Nature (London)* **354**, 445 (1991).
- <sup>2</sup>S. C. Moss and D. L. Price, in *Physics of Disordered Materials*, edited by D. Adler, H. Fritzsche, and S. R. Ovshinsky (Plenum, New York, 1985), p. 77.
- <sup>3</sup>D. L. Price, S. C. Moss, R. Reijers, M. L. Saboungi, and S. Susman, *J. Phys. C* **21**, L1069 (1988).
- <sup>4</sup>S. R. Elliott, *Phys. Rev. Lett.* **67**, 711 (1991).
- <sup>5</sup>R. J. Nemanich, S. A. Solin, and G. Lucovsky, *Solid State Commun.* **21**, 273 (1977).
- <sup>6</sup>P. M. Bridenbaugh, G. P. Espinosa, J. E. Griffiths, J. C. Phillips, and J. P. Remeika, *Phys. Rev. B* **20**, 4140 (1979).
- <sup>7</sup>W. J. Bresser, P. Boolchand, P. Suranyi, and J. P. de Neufville, *Phys. Rev. Lett.* **46**, 1689 (1981).
- <sup>8</sup>P. Boolchand, J. Grothaus, W. J. Bresser, and P. Suranyi, *Phys. Rev. B* **25**, 2975 (1982).
- <sup>9</sup>K. Murase, T. Fukunaga, K. Yakushiji, T. Yoshimi, and I. Yunoki, *J. Non-Cryst. Solids* **59-60**, 883 (1983).
- <sup>10</sup>R. J. Nemanich, F. L. Galeener, J. C. Mikkelsen, G. A. N. Connell, G. Etherington, A. C. Wright, and R. N. Sinclair, *Physica B* **117&118**, 959 (1983).
- <sup>11</sup>X. Sugai, *Phys. Rev. B* **35**, 1345 (1987).
- <sup>12</sup>I. Petri, P. S. Salmon, and H. E. Fischer, *Phys. Rev. Lett.* **84**, 2413 (2000).
- <sup>13</sup>P. Boolchand and W. J. Bresser, *Philos. Mag. B* **80**, 1757 (2000).
- <sup>14</sup>S. Susman, K. J. Volin, D. G. Montague, and D. L. Price, *J. Non-Cryst. Solids* **125**, 168 (1990).
- <sup>15</sup>P. Vashishta, R. K. Kalia, G. A. Antonio, and I. Ebbsjö, *Phys. Rev. Lett.* **62**, 1651 (1989).
- <sup>16</sup>P. Vashishta, R. K. Kalia, and I. Ebbsjö, *Phys. Rev. B* **39**, 6034 (1989).
- <sup>17</sup>H. Iyetomi, P. Vashishta, and R. K. Kalia, *Phys. Rev. B* **43**, 1726 (1991).
- <sup>18</sup>P. Vashishta, R. K. Kalia, J. P. Rino, and I. Ebbsjö, *Phys. Rev. B* **41**, 12 197 (1990).
- <sup>19</sup>I. T. Penfold and P. S. Salmon, *Phys. Rev. Lett.* **67**, 97 (1991).
- <sup>20</sup>A. Bhatia and D. Thornton, *Phys. Rev. B* **2**, 3004 (1970).
- <sup>21</sup>C. Massobrio, A. Pasquarello, and R. Car, *Phys. Rev. Lett.* **80**, 2342 (1998).
- <sup>22</sup>C. Massobrio, A. Pasquarello, and R. Car, *J. Am. Chem. Soc.* **121**, 2943 (1999).
- <sup>23</sup>R. Car and M. Parrinello, *Phys. Rev. Lett.* **55**, 2471 (1985).
- <sup>24</sup>D. M. Ceperley and B. J. Alder, *Phys. Rev. Lett.* **45**, 566 (1980).
- <sup>25</sup>J. P. Perdew and A. Zunger, *Phys. Rev. B* **23**, 5048 (1981).
- <sup>26</sup>J. P. Perdew, J. A. Chevary, S. H. Vosko, K. A. Jackson, M. R. Pederson, D. J. Singh, and C. Fiolhais, *Phys. Rev. B* **46**, 6671 (1992).
- <sup>27</sup>R. Stumpf, X. Gonze, and M. Scheffler (unpublished); see also X. Gonze, R. Stumpf, and M. Scheffler, *Phys. Rev. B* **44**, 8503 (1991).
- <sup>28</sup>A. Dal Corso, A. Pasquarello, A. Baldereschi, and R. Car, *Phys. Rev. B* **53**, 1180 (1996).
- <sup>29</sup>K. P. Huber and G. Herzberg, *Molecular Spectra and Molecular Structure, IV. Constants of Diatomic Molecules* (Van Nostrand, Princeton, 1979).
- <sup>30</sup>C. Massobrio, A. Pasquarello, and R. Car, *Comput. Mater. Sci.* **17**, 115 (2000).
- <sup>31</sup>F. Tassone, F. Mauri, and R. Car, *Phys. Rev. B* **50**, 10 561 (1994).
- <sup>32</sup>S. Nosé, *Mol. Phys.* **52**, 255 (1984); W. G. Hoover, *Phys. Rev. A* **31**, 1695 (1985).
- <sup>33</sup>P. Blöchl and M. Parrinello, *Phys. Rev. B* **45**, 9413 (1992).
- <sup>34</sup>A. Pasquarello, K. Laasonen, R. Car, C. Lee, and D. Vanderbilt, *Phys. Rev. Lett.* **69**, 1982 (1992).
- <sup>35</sup>K. Laasonen, A. Pasquarello, R. Car, C. Lee, and D. Vanderbilt, *Phys. Rev. B* **47**, 10 142 (1993).
- <sup>36</sup>For the explicit relationship between the three sets of partial structure factors commonly used [Faber-Ziman, Ashcroft-Langreth, and Bhatia-Thornton (Ref. 20); see Y. Waseda, *The Structure of Non-Crystalline Materials* (McGraw-Hill, New York, 1980)].
- <sup>37</sup>P. S. Salmon, *Proc. R. Soc. London, Ser. A* **437**, 591 (1992).
- <sup>38</sup>I. Petri, Ph.D. thesis, University of Bath, 1999; P. S. Salmon (unpublished results).
- <sup>39</sup>I. Petri, P. S. Salmon, and W. S. Howells, *J. Phys.: Condens. Matter* **11**, 10 219 (1999).
- <sup>40</sup>C. Massobrio, F. H. M. van Roon, A. Pasquarello, and S. W. de Leeuw, *J. Phys.: Condens. Matter* **12**, L697 (2000).
- <sup>41</sup>M. Cobb and D. A. Drabold, *Phys. Rev. B* **56**, 3054 (1997).
- <sup>42</sup>F. H. M. van Roon, C. Massobrio, E. de Wolff, and S. W. de Leeuw, *J. Chem. Phys.* **113**, 5425 (2000).
- <sup>43</sup>G. Kresse and J. Hafner, *Phys. Rev. B* **49**, 14 251 (1994).
- <sup>44</sup>R. V. Kulkarni, W. G. Aulbur, and D. Stroud, *Phys. Rev. B* **55**, 6896 (1997).
- <sup>45</sup>P. S. Salmon, *J. Phys. F: Met. Phys.* **18**, 2345 (1988).
- <sup>46</sup>J. P. Gabathuler and S. Steeb, *Z. Naturforsch. A* **34**, 1314 (1979).
- <sup>47</sup>D. S. Franzblau, *Phys. Rev. B* **44**, 4925 (1991).
- <sup>48</sup>V. Rosato, M. Celino, G. Benedek, and S. Gaito, *Phys. Rev. B* **60**, 16 928 (1999).
- <sup>49</sup>J. Peters and B. Krebs, *Acta Crystallogr., Sect. B: Struct. Crystallogr. Cryst. Chem.* **38**, 1270 (1982).
- <sup>50</sup>G. Dittmar and H. Schäfer, *Acta Crystallogr., Sect. B: Struct. Crystallogr. Cryst. Chem.* **32**, 2726 (1976).
- <sup>51</sup>G. Galli and M. Parrinello, *J. Chem. Phys.* **95**, 7504 (1991).
- <sup>52</sup>Q. M. Zhang, G. Chiarotti, A. Selloni, R. Car, and M. Parrinello, *Phys. Rev. B* **42**, 5071 (1990).
- <sup>53</sup>J. Sarnthein, A. Pasquarello, and R. Car, *Phys. Rev. Lett.* **74**, 4682 (1995); *Phys. Rev. B* **52**, 12 690 (1995).
- <sup>54</sup>G. A. de Wijs, G. Pastore, A. Selloni, and W. van der Lugt, *Phys. Rev. B* **48**, 13 459 (1993).

- <sup>55</sup>G. Kresse and J. Hafner, Phys. Rev. B **49**, 14 251 (1994).
- <sup>56</sup>F. Kirchoff, J. M. Holender, and M. J. Gillan, Phys. Rev. B **54**, 190 (1996).
- <sup>57</sup>G. A. de Wijs, G. Pastore, A. Selloni, and W. van der Lugt, J. Phys.: Condens. Matter **8**, 1879 (1996).
- <sup>58</sup>F. Shimojo, S. Munejiri, K. Hoshino, and Y. Zempo, J. Phys.: Condens. Matter **11**, L153 (1999).
- <sup>59</sup>K. Seifert-Lorenz and J. Hafner, Phys. Rev. B **59**, 843 (1999).
- <sup>60</sup>R. V. Kulkarni and D. Stroud, Phys. Rev. B **62**, 4991 (2000).
- <sup>61</sup>R. W. Impey, P. A. Madden, and I. R. McDonald, J. Phys. Chem. **87**, 5071 (1983).
- <sup>62</sup>U. Walter, D. L. Price, S. Susman, and K. J. Volin, Phys. Rev. B **37**, 4232 (1989).
- <sup>63</sup>W. H. Zachariasen, J. Am. Chem. Soc. **54**, 3841 (1932).
- <sup>64</sup>I. T. Penfold and P. S. Salmon, Phys. Rev. Lett. **68**, 253 (1992); P. Boolchand and J. C. Phillips, *ibid.* **68**, 252 (1992).